Laser spectroscopic studies of the pure rotational $U_0(0)$ and $W_0(0)$ transitions of solid parahydrogen

Man-Chor Chan, Szetsen S. Lee, Mitchio Okumura,[a] and Takeshi Oka
Department of Chemistry and Department of Astronomy and Astrophysics, The University of Chicago, Chicago, Illinois 60637

(Received 8 March 1991; accepted 28 March 1991)

High resolution spectrum of multipole-induced transitions of solid parahydrogen was recorded using diode and difference frequency laser spectroscopy. The $J = 4 \leftarrow 0$ pure rotational $U_0(0)$ transition observed in the diode spectrum agrees well in frequency with the value reported by Balasubramanian *et al.* [Phys. Rev. Lett. **47**, 1277 (1981)] but we observed a spectral width smaller by about a factor of 4. The $J = 6 \leftarrow 0$ $W_0(0)$ transition was observed to be exceedingly sharp, with a width of ~ 70 MHz, using a difference frequency spectrometer with tone-burst modulation. This transition is composed of three components with varying relative intensity depending upon the direction of polarization of laser radiation. These components were interpreted as the splitting of the M levels in the $J = 6$ state due to crystal field interactions. In addition, a new broad feature was found at 2452.4 cm^{-1} in the low resolution Fourier-transform infrared (FTIR) spectrum of solid hydrogen and was assigned to be the phonon branch $W_R(0)$ transition of the $W_0(0)$ line. The selection rules, crystal field splitting of $J = 4$ and $J = 6$ rotons, and the measured linewidth based on these observations are discussed.

I. INTRODUCTION

Hydrogen forms the simplest and most fascinating molecular solid. H_2 molecules are held together to form the hexagonal close-packed (hcp) structure mainly by long range dispersion interactions.[1] Since the neighboring intermolecular separation (3.793 Å) is much larger than the internuclear distance of the molecule (0.741 Å), hydrogen molecules are only slightly perturbed in solid state and most of the solid properties can be calculated from first principles.[2] As a result of weak intermolecular interactions and small molecular mass, the properties of solid hydrogen are dominated by quantum effects.[2,3] Together with helium, solid hydrogens (H_2 and its isotopic species) are categorized as quantum crystals.[4] The amplitude of zero-point lattice vibration is a significant fraction of the intermolecular distance ($\sim 18\%$ for H_2) in these systems leading to the failure of harmonic approximation.[4] Compared with helium, solid hydrogens are more attractive to spectroscopists because various molecular motions, including rotation, vibration and electronic motion of hydrogen molecules in the solid state provide a rich spectrum over a wide spectral region.

The pure rotational and rovibrational transitions of gaseous H_2 are strictly dipole forbidden. However, solid hydrogen absorbs strongly from far infrared to near infrared. The initial spectroscopic work of its fundamental band by Allin, Hare, and MacDonald[5] in 1955 provided clear evidence for the nearly free rotation and vibration of H_2 molecules in the solid state.[5,6] The resemblance of the rovibrational pattern in the solid spectrum to that of gas phase molecules indicated that the rotational quantum number J and vibrational quantum number v of molecular hydrogens remain good quantum numbers in condensed phases. By extending the idea of collision-induced absorptions of gas molecules under high pressure,[7] Van Kranendonk developed a theory to explain the solid spectrum.[8,9] The multipole moment of each hydrogen molecule induces coherent dipole moments in the surrounding molecules and these dipole moments cause the absorption of photon through many-body radiative interactions.[2] The selection rules of these induced features therefore follow those of multipole transitions and the intensities of spectral lines due to various induction mechanisms are determined by the strength of the interactions. Since the induced dipole is a collective property of the crystal depending on intermolecular interaction and the excitation and relaxation processes involve many-body interactions, the properties of the molecule and those of the crystal have to be simultaneously considered in treating various aspects of spectroscopy such as selection rules, relative intensities, transition frequencies, etc. This makes the spectroscopy of solid hydrogen qualitatively different from the conventional spectroscopy of gaseous molecules where in the latter only an isolated molecule and its interaction with radiation are considered.

Since the observation of the earliest spectrum of the rovibrational Q and S branches,[5] the $\Delta J = 4$ hexadecapole-induced $U_{1\leftarrow 0}(J)$ lines[10] and the $\Delta J = 6$ tetrahexacontapole (64-pole)-induced $W_{1\leftarrow 0}(0)$ transition[11] have also been reported. Kiss started the studies of the pure rotational transitions by observing the $S_0(0)$ transition.[12] Treffler, Cappel, and Gush improved the resolution of the spectrum in 1969.[13] Buontempo, Cunsolo, Dore, and Nencini reported the spectrum of the $S_0(1)$ transition in 1982.[14] Balasubramanian, Lien, Rao, and Gaines[15] observed the $U_0(0)$ and $U_0(1)$ transitions in 1981 while the much weaker $W_0(0)$ transition[11] has been reported recently.

Most of the observed zero-phonon single transitions are sharp in nearly pure $J = 0$ solid. In particular, our preliminary studies of the $W_0(0)$ transition of solid p-H_2 using a difference frequency spectrometer have revealed that this

[a] Present address: Division of Chemistry, California Institute of Technology, Pasadena, CA 91125.

 0021-9606/91/130088-10$03.00

transition has a spectral width of 0.003 cm^{-1} (90 MHz) corresponding to a spectral resolution of $\Delta\nu/\nu \sim 10^{-6}$,[11] more than an order of magnitude smaller than the typical Doppler-limited linewidth of gas phase transitions. A rich spectrum composed of hundreds of lines with even smaller width ($\sim$20 MHz, corresponding to $\Delta\nu/\nu \sim 10^{-7}$) was observed in the fundamental Q branch of 99.8% p-H_2 samples.[16] These observations set an upper limit of the inhomogeneous broadening in our samples to be $\lesssim$20 MHz.

High resolution spectroscopy allows us to observe intricate features in the spectrum of solid H_2, which may lead us to a better understanding of the structure and dynamics of this "simple" molecular solid. These spectra provide information on intermolecular interactions as well as radiative and relaxational processes in the solid phase. In this paper, we report our studies of the $U_0(0)$ transitions using diode laser spectroscopy and observations of the pure rotational W branch using Fourier transform infrared (FTIR) and difference frequency spectroscopy.

II. THEORETICAL ASPECTS

A. Symmetry and selection rules

The degeneracy of the M sublevels in the J manifold of a molecule is removed in solid state due to the finite symmetry of crystal environment. The qualitative discussion of the splitting and selection rules depends on the symmetry of the molecule as well as that of the crystal. Based on the theory of permutation–inversion group of Hougen[17] and Longuet-Higgins,[18] Miller and Decius developed a theoretical treatment for molecules isolated in solid matrices using an extended group to include both molecular and crystal symmetry.[19] In this section we will apply this theory to solid hydrogen.

The molecular symmetry group $\mathscr{M}$ of an H_2 molecule is composed of four elements,

$$\mathscr{M} = \{\overline{E}, (\overline{12}), \overline{E}^*, (\overline{12})^*\}.$$

$\overline{E}$ and $(\overline{12})$ are identity and permutation of the two protons, respectively, and operations with asterisks are operations with permutation followed by the space inversion $\overline{E}^*$. We follow the convention of Miller and Decius to use permutation–inversion group notation with overbars for operations in $\mathscr{M}$.[19] The point group $\mathscr{S}$ of solid H_2 with the hcp structure is D_{3h},

$$\mathscr{S} = \{E, 2C_3, 3C_2, \sigma_h, 2S_3, 3\sigma_v\},$$

where the symbol of each operation is written in the standard point group notation.[20] The appropriate extended group $\mathscr{G}$ for an H_2 molecule embedded in an hcp crystal is composed of the "feasible" operations in the direct product group of $\mathscr{M}$ and $\mathscr{S}$.[19] The group $\mathscr{G}$ is composed of 24 elements and is isomorphic to D_{6h}. Table I lists the character table of $\mathscr{G}$. The symmetry classifications of the crystal-fixed components of the dipole moment μ and the polarizability tensor α are also given in Table I.

For determining the symmetry representations of the rotational levels, we use the following symmetry relations:

$$\begin{aligned}
&\overline{E}^*|J,M\rangle = (-1)^J|J,M\rangle,\\
&(\overline{12})|J,M\rangle = (-1)^J|J,M\rangle,\\
&C_3|J,M\rangle = e^{2\pi iM/3}|J,M\rangle,\\
&C_2|J,M\rangle = (-1)^{J+M}|J,-M\rangle,\\
&\sigma_h|J,M\rangle = (-1)^{J+M}|J,M\rangle.
\end{aligned} \tag{1}$$

These relations can be obtained by considering the change of polar angles of spherical harmonics under each symmetry operation. For the C_2 operation, the choice of rotation with respect to x or y axis is arbitrary.[17,21] We use a convention of C_{2y}.[21] If C_{2x} is used, the relation will be[17]

$$C_2|J,M\rangle = (-1)^J|J,-M\rangle$$

and the scheme of symmetry classification will be different. However, the choice of C_2 axis does not affect the final results. The general scheme of symmetry classification of rotational wave functions based on Eq. (1) is listed in Table II. It is straightforward to show from Tables I and II that the $J = 2 \leftarrow 0$ transition of solid H_2 is composed of three peaks in the Raman spectrum but only one single component in the infrared spectrum as observed in experiments.[12–14,22]

Both $U_0(0)$ and $W_0(0)$ transitions have three infrared active components corresponding to $|M| = 2$, 3, and 4, respectively, in the excited state. The dipole moment μ_0 gives rise to the $|M| = 3 \leftarrow 0$ transition and $\mu_{\pm 1}$ give rise to the $|M| = 2 \leftarrow 0$ and $4 \leftarrow 0$ transitions. These results can also be

TABLE I. Character table of group $\mathscr{G}$.

$\mathscr{G}$	$E\overline{E}$	$2C_3\overline{E}$	$3C_2\overline{E}$	$E(\overline{12})$	$2C_3(\overline{12})$	$3C_2(\overline{12})$	$\sigma_h\overline{E}^*$	$2S_3\overline{E}^*$	$3\sigma_v\overline{E}^*$	$\sigma_h(\overline{12})^*$	$2S_3(\overline{12})^*$	$3\sigma_v(\overline{12})^*$		
sA_1'	1	1	1	1	1	1	1	1	1	1	1	1		$\alpha_{zz}, \alpha_{xx}+\alpha_{yy}$
sA_2'	1	1	−1	1	1	−1	1	1	−1	1	1	−1		
sE'	2	−1	0	2	−1	0	2	−1	0	2	−1	0	(μ_{+1}, μ_{-1})	$(\alpha_{xx}-\alpha_{yy}, \alpha_{xy})$
aA_1'	1	1	1	−1	−1	−1	1	1	1	−1	−1	−1		
aA_2'	1	1	−1	−1	−1	1	1	1	−1	−1	−1	1		
aE'	2	−1	0	−2	1	0	2	−1	0	−2	1	0		
sA_1''	1	1	1	1	1	1	−1	−1	−1	−1	−1	−1		
sA_2''	1	1	−1	1	1	−1	−1	−1	1	−1	−1	1	μ_0	
sE''	2	−1	0	2	−1	0	−2	1	0	−2	1	0		$(\alpha_{xz}, \alpha_{yz})$
aA_1''	1	1	1	−1	−1	−1	−1	−1	−1	1	1	1		
aA_2''	1	1	−1	−1	−1	1	−1	−1	1	1	1	−1		
aE''	2	−1	0	−2	1	0	−2	1	0	2	−1	0		

TABLE II. Classification of rotational wave functions in group $\mathscr{S}$.

Rotational quantum number		Symmetry
J even		s
J odd		a
$M=0$	J even	sA_1'
	J odd	aA_2'
$M\neq 0$	$\lvert M\rvert = 0 \pmod 6$	aA_2'
	$\lvert M\rvert = 1 \pmod 6$	E''
	$\lvert M\rvert = 2 \pmod 6$	E'
	$\lvert M\rvert = 3 \pmod 6$	aA_2'
	$\lvert M\rvert = 4 \pmod 6$	E'
	$\lvert M\rvert = 5 \pmod 6$	E''

obtained by considering the scheme of angular momentum coupling among the induced dipole moment and rotational states.[23] Nevertheless, the group theoretical consideration is transparent and straightforward.

B. Crystal field splitting

The splitting of the $|J,M\rangle$ levels results from two effects: (1) dynamic hopping of the rotational excitation and (2) static crystal field interactions. We will discuss their magnitudes for different rotational states.

The excitation energy introduced to a molecule after the absorption of a photon can hop around in the crystal through interactions between nearby molecules and behaves as a traveling wave (exciton) characterized by a wave vector k. Exciton bands composed of excitons with various values of k are formed in the solid state as a result of the removal of the degeneracy due to intermolecular interactions. The rotational exciton is called a roton. The rotational excitation from the $J=0$ state is limited to $\mathbf{k}\approx 0$ rotons by selection rule.[2]

The M splitting of the $\mathbf{k}\approx 0$ roton band was first calculated by Van Kranendonk.[2,8,9] He applied a delocalized roton model to interpret the triplet structure of the $S_0(0)$ Raman line as the M splitting of the $\mathbf{k}\approx 0$ levels in the $J=2$ roton band due to resonance hopping of the rotational energy by anisotropic electrostatic quadrupole–quadrupole (EQQ) interactions between molecules. This model successfully explained the Raman splitting of $\sim 2\ \mathrm{cm}^{-1}$ between each component.[22]

In the case of a roton band with J higher than 2, the resonance hopping becomes much slower because of weaker interactions. For instance, the hopping of the $J=4$ and $J=6$ rotons involves hexadecapole–hexadecapole and tetrahexacontapole–tetrahexacontapole interactions, respectively. A quantitative expression for the interaction energy $\mathscr{V}_{l_1 l_2}$ between multipole moments $Q^{(l_1)}$ and $Q^{(l_2)}$ can be written as[24–29]

$$\mathscr{V}_{l_1 l_2} = \varepsilon_{l_1 l_2} \sum_{mn} C(l_1 l_2 l_1 + l_2; mnm+n) C_{l_1 m}(\mathbf{\Omega}_1) \times C_{l_2 n}(\mathbf{\Omega}_2) C^*_{l_1+l_2, m+n}(\mathbf{\Omega}_{12}), \tag{2}$$

where

$$\varepsilon_{l_1 l_2} = (-1)^{l_2} \left[\frac{(2l_1+2l_2)!}{(2l_1)!(2l_2)!}\right]^{1/2} \frac{Q^{(l_1)} Q^{(l_2)}}{R^{l_1+l_2+1}}. \tag{3}$$

$Q^{(l_1)}$ and $Q^{(l_2)}$ represent the two interacting multipole moments of order l_1 and l_2, respectively, R is the distance between the two multipole moments, and $\mathbf{\Omega}_1$, $\mathbf{\Omega}_2$, and $\mathbf{\Omega}_{12}$ are the orientation of $Q^{(l_1)}$, $Q^{(l_2)}$ and $\mathbf{R}$, respectively. To estimate the order of the magnitude of the interactions, we compare the coupling constants $\varepsilon_{l_1 l_2}$'s of quadrupole–quadrupole, hexadecapole–hexadecapole, and tetrahexacontapole–tetrahexacontapole interactions,

$$\varepsilon_{22}:\varepsilon_{44}:\varepsilon_{66} \sim \frac{e^2 a_0^4}{R_0^5}:\frac{e^2 a_0^4}{R_0^5}\left(\frac{a_0}{R_0}\right)^4:\frac{e^2 a_0^4}{R_0^5}\left(\frac{a_0}{R_0}\right)^8 \sim 1:3\times 10^{-4}:10^{-7}.$$

e, R_0, and a_0 are the electronic charge, the nearest-neighbor distance of solid H_2 (3.793 Å) and the Bohr radius (0.529 Å), respectively. Taking the splitting of the infrared active $\mathbf{k}\approx 0$ roton in the $J=2$ band to be $\sim 10\ \mathrm{cm}^{-1}$,[2] we estimate the splitting of the $U_0(0)$ and $W_0(0)$ transitions due to roton hopping to be on the order of 0.003 and 0.000 001 cm^{-1}, respectively.

The slow hopping of the $J=4$ and $J=6$ rotons suggests that the excitation energy localizes on a particular molecule for appreciably long time. Under this situation, the effect of static interactions of the localized roton with the crystal environment becomes dominant for producing the M splitting of highly excited rotational states. Assuming that the rotational excitation energy is localized on the central molecule, we can calculate the effect of crystal field on the M levels in the J manifold using the same theoretical treatment for the case of a single $J=1$ molecule in an otherwise $J=0$ solid.[2,30,31] The permanent quadrupole moment of the excited molecule produces dipole moments on the surrounding molecules with isotropic polarizability α, and these dipole moments in turn interact with the quadrupole field to produce excess binding energy. The total polarization energy $\mathscr{E}_{\mathrm{pol}}$ summing over the crystal is given by[2]

$$\mathscr{E}_{\mathrm{pol}} = \frac{105}{2}\frac{\alpha Q^2}{R_0^8} \sum_{l=0,2,4} \begin{Bmatrix} 3 & 3 & l \\ 2 & 2 & 1 \end{Bmatrix} C(22l;000) C(33l;000) \times \sum_m (-1)^m C_{lm}(\mathbf{\Omega}) \sum_\rho{}' \left[\frac{R_0}{R_\rho}\right]^8 C_{l\bar{m}}(\mathbf{\Omega}_\rho). \tag{4}$$

$\mathbf{R}_\rho = (R_\rho, \mathbf{\Omega}_\rho)$ is the position vector of the molecule ρ from the central molecule, Ω is the orientation of the central molecule, and $Q \equiv |\langle v=0, J|Q^{(2)}|v=0, J\rangle|$ is the permanent quadrupole moment of the excited molecule in J state. The splitting due to this effect has a similar order of magnitude for rotons with $J=2$, 4, 6, etc. and it becomes dominant for rotons with J higher than 4, as we will discuss below.

In order for the lattice sum Σ' in Eq. (4) to be nonvanishing, it has to be invariant under all operations in group $\mathscr{S}$. The Racah spherical harmonics C_{lm} transform like rotational wave functions $|l,m\rangle$. Expressing $\mathbf{R}_\rho$ and $\mathbf{\Omega}$ in the crystal frame and using the relations in Eq. (1), we see that $m=3k$ (from C_3) and m has to be even (from σ_h). Combining both conditions, only $m=0$ has a nonzero crystal sum and contributes to $\mathscr{E}_{\mathrm{pol}}$. We can rewrite Eq. (4) in the form

$$\mathscr{E}_{\mathrm{pol}} = \varepsilon_{2c} C_{20}(\mathbf{\Omega}) + \varepsilon_{4c} C_{40}(\mathbf{\Omega}), \tag{5}$$

TABLE III. Orders of magnitude[a] of coupling constants for delocalized and localized rotons.

	Delocalized roton		Localized roton	
J	Coupling constant	Order of magnitude	Coupling constant	Order of magnitude
2	ε_{22}	$e^2a_0^4R_0^{-5}$	$\varepsilon_{2c},\varepsilon_{4c}$	$e^2a_0^7R_0^{-8}$
4	ε_{44}	$e^2a_0^8R_0^{-9}$	$\varepsilon_{2c},\varepsilon_{4c}$	$e^2a_0^7R_0^{-8}$
6	ε_{66}	$e^2a_0^{12}R_0^{-13}$	$\varepsilon_{2c},\varepsilon_{4c}$	$e^2a_0^7R_0^{-8}$

[a]The coupling constants are expressed in terms of energy, where e, a_0, and R_0 are the electronic charge, the Bohr radius (0.529 Å), and the nearest intermolecular separation of solid H_2 (3.793 Å), respectively.

where

$$\varepsilon_{lc}=\frac{105}{2}\frac{\alpha Q^2}{R_0^8}\begin{Bmatrix}3 & 3 & l\\ 2 & 2 & 1\end{Bmatrix}C(22l;000)C(33l;000)\times\sum_{\rho}{}'\left[\frac{R_0}{R_\rho}\right]^8 C_{l0}(\Omega_\rho). \quad (6)$$

The term with $l=0$ is dropped because it has no angular dependence and only shifts the origin of the transition frequency. The coupling constant ε_{lc} is on the order of $\alpha QR_0^{-8}\sim 0.044\ \mathrm{cm}^{-1}$ (1.3 GHz). Table III shows a comparison of the magnitudes of the coupling constants of resonance hopping in delocalized roton model and static crystal field effect of localized roton for $J=2$, 4, and 6 bands. For the $J=2$ band, the delocalized roton model gives much larger splitting, whereas for $J=4$ and 6 bands, the static crystal field effect gives larger splitting. The M splitting of the $U_0(0)$ and $W_0(0)$ transitions is therefore ascribed mostly to the crystal field interactions of the localized rotons.

Using Eq. (6) and assuming a rigid hcp structure, the coupling constants ε_{2c} and ε_{4c} were calculated to be $-9.03\times10^{-5}\ \mathrm{cm}^{-1}$ and $-0.0595\ \mathrm{cm}^{-1}$, respectively. In summing the lattice effect, 20 shells of neighbors were taken into account with good convergence. ε_{2c} is very small because contributions from the first two shells accidentally vanish for hcp structure.[2]

Anisotropic dispersion interaction also contributes to the M splitting. This effect can be calculated by transforming the general form of the anisotropic pair potential[2,32]

$$A(\omega)=-\sum_{n=6,8,10}\frac{b_n}{R^n}C_{20}(\omega)-\sum_{n=8,10}\frac{c_n}{R^n}C_{40}(\omega) \quad (7)$$

into the crystal-fixed frame and then summing over the crystal. The general expression of the splitting Hamiltonian can be written as

$$\mathscr{H}_c=-C_{20}(\Omega)\sum_{n=6,8,10}\frac{b_n}{R_0^n}\sum_{\rho}{}'\left(\frac{R_0}{R_\rho}\right)^n C_{20}(\Omega_\rho)-C_{40}(\Omega)\sum_{n=8,10}\frac{c_n}{R_0^n}\sum_{\rho}{}'\left(\frac{R_0}{R_\rho}\right)^n C_{40}(\Omega_\rho). \quad (8)$$

Again the contribution from the b_n's in Eq. (8) almost completely disappears in the lattice sum. Both induction and dispersion effects contribute to b_n and c_n which can be determined separately by *ab initio* calculations.[2,32] According to the calculations of Mulder, Van der Avoird, and Wormer,[32] the effect of dispersion is far more important than that of induction for splitting terms with $C_{20}(\Omega)$ dependence. On the other hand, both induction and dispersion have comparable contributions to terms with $C_{40}(\Omega)$ dependence. Using the *ab initio* results of Mulder *et al.*[32] and Meyer,[33] Van Kranendonk[34] calculated the coefficients in Eqs. (7) and (8), for combined dispersion and induction effects, to be $b_6=1.368$ a.u., $b_8=50.53$ a.u., $b_{10}=1185.0$ a.u., $c_8=2.44$ a.u., and $c_{10}=46.3$ a.u., respectively. Using these values in Eq. (8), the splitting Hamiltonian can be written as

$$\mathscr{H}_c(\text{in cm}^{-1})=-0.000\,26C_{20}(\Omega)-0.113C_{40}(\Omega). \quad (9)$$

The effect of electron overlap in producing the anisotropic potential was expected to be negligible based on the calculations of Ng, Meath, and Allnatt.[35] They found that at $R\gtrsim 7\ a_0(\sim 3.7$ Å), the correction of EQQ interaction due to charge overlap is about 0.2%. The contribution of overlap to other higher order interactions is expected to be even smaller at this separation. In practice various corrections should be considered when using these coupling constants for solid hydrogen, which will be discussed in Sec. VI.

It is seen from Eq. (9) and the matrix element of $C_{40}(\Omega)$ that the energies of the three infrared allowed states in the excited rotational levels decrease with decreasing $|M|$ value. Our assignment is partly based on this phenomenon. The combined contribution of induction and dispersion effects discussed above gives splitting which agrees well with the observed value.

III. EXPERIMENT

The cryostat used was modified from a commercial Infrared Laboratories HD-3 helium Dewar. A copper sample cell was mounted on the cold surface of the Dewar. The cell was thus kept at or close to 4.2 K when the spectra were taken. Two cells with 1.0 and 11.5 cm path length, respectively, were used. The short cell sealed with CsI windows was used for the $U_0(0)$ transition whereas the long cell fitted with sapphire windows was used for the $W_0(0)$ and $W_R(0)$ lines.

Ultrahigh purity (>99.9995%) normal hydrogen gas from Matheson was passed through a column of Appachi catalyst maintained at ~18–20 K, in a liquid H_2 bath, to convert to ~99.94–99.8% para-enriched gas. This temperature range was achieved by slowly pumping the bath to reduce the vapor pressure. The o-H_2 concentration in the outcoming para-enriched gas was determined by the integrated absorption intensity of the corresponding $Q_{1\leftarrow0}(1)$ transition. Solid H_2 sample was prepared by pulsing the para-enriched gas into the sample cell at a pressure of ~50–100 Torr to maintain approximately constant temperature (estimated to be below 10 K).[11] Samples prepared by this method are normally optically transparent. Examinations of the samples through crossed polarizers show that our samples do not have grain boundaries but have some mechanical strains. However the reproducibility of the spectrum for probing different parts of the sample and different samples suggests that the optical quality of the crystals is constant.

A diode laser spectrometer with spectral purity of 0.0003 cm^{-1} ($\sim$10 MHz) was used to study the $U_0(0)$ transition. The laser source was frequency modulated at about 10 kHz. The infrared signal was detected using a liquid N_2 cooled HgCdTe detector and processed through a phase sensitive detector using $2f$ signal detection. The frequency was measured against N_2O reference absorptions.[36] The uncertainty in frequency measurement is about 0.005 cm^{-1} restricted by the linearity of the etalon fringes with a free spectral range of 0.048 cm^{-1}.

The low resolution (at 4 cm^{-1}) spectrum of the $W_R(0)$ transition was recorded using a Fourier transform spectrometer with a globar source and a CaF_2 beam splitter. The optical path was purged with N_2 gas to minimize the background absorptions due to atmospheric H_2O and CO_2.

The high resolution spectrum of the $W_0(0)$ transition was recorded using a difference frequency spectrometer.[37] Tunable narrow-band infrared radiation with spectral purity of $\lesssim$2 MHz was generated in a $LiNbO_3$ crystal by nonlinear mixing of the output of a cw single mode ring dye laser with the 514 nm line of a single mode cw argon ion laser. The laser light was tone-burst modulated[38] at 6 kHz. High power radio frequency (RF) radiation of 40 MHz was used to generate RF sidebands to the 514 nm line in an electro-optical KDP (potassium dihydrogen phosphate, KH_2PO_3) crystal to produce RF sidebands prior to the infrared generation. The power of each sideband was about 30% of the Ar emission intensity. These sidebands were transferred to the infrared after difference frequency mixing. The RF source was amplitude modulated with a square wave at 6 kHz through a double balanced mixer and consequently the sidebands were turned on and off at a frequency of 6 kHz. The signal was detected by a liquid N_2 cooled InSb detector and processed through a phase sensitive detector referenced at 6 kHz. This modulation technique gives a second derivative spectrum. The infrared frequency was calibrated by reference absorptions of N_2O gas. The uncertainty in absolute frequency measurement is about 0.0020 cm^{-1} limited by the accuracy of the measurements of reference absorptions, although the resolution and the accuracy of the relative frequency measurements are much better, on the order of 0.0005 cm^{-1}.

IV. OBSERVATIONS

A. $U_0(0)$ transition

Figure 1 shows the $U_0(0)$ transition in a sample of 1 cm long solid p-H_2 with $\sim$0.2% o-H_2 impurity recorded by the diode spectrometer. The transition frequency was measured to be 1167.1139 cm^{-1} with $\sim$75% absorption, consistent with the previous measurement at 1167.10 cm^{-1} by Balasubramanian *et al.*[15] Our measured linewidth (HWHM) was 0.03 cm^{-1}, about four times smaller than that obtained in the previous work. Since both spectra were recorded at different temperatures (The spectrum of Balasubramanian *et al.* was recorded at 13 K whereas our spectrum was recorded at $\sim$4.2 K.), the discrepancy in the linewidth measurement may be due to the temperature dependence of spectral width. The inhomogeneous broadening may also be different for different samples. The major inhomogeneous broadening comes from the mechanical strains resulting from the different thermal expansion between solid H_2 and the sample cell material. However, no quantitative model on strain broadening has been reported.

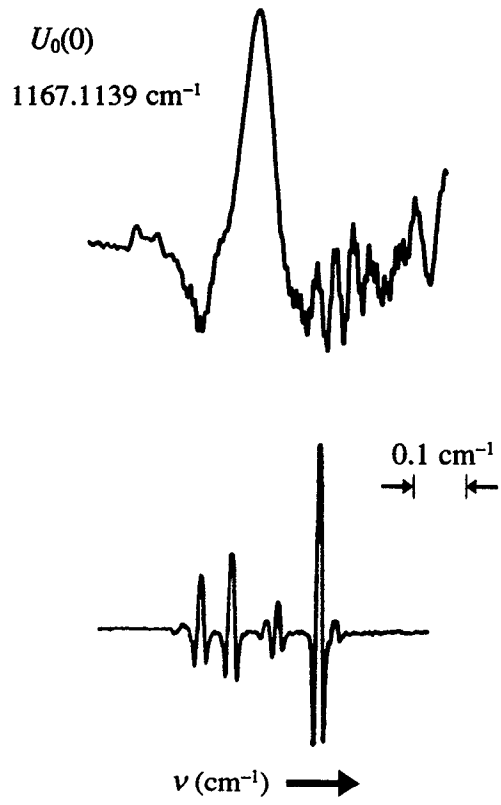

FIG. 1. Diode laser spectrum (upper trace) of the $U_0(0)$ transition at 1167.1139 cm^{-1} with spectral width HWHM 0.03 cm^{-1}. The optical path is 1 cm, and the sample contains $\sim$0.2% of o-H_2. The lower trace is the N_2O reference absorptions. Frequency modulation at 10 kHz with $2f$ detection and 3 s time constant were used. The noise at the high frequency side of the line is due to diode quality.

B. Phonon associated $W_R(0)$ transition

In addition to the zero-phonon lines due solely to molecular excitation, double transitions involving simultaneous excitation of a molecule and lattice vibration (phonon) by absorbing a single photon can also occur in solid materials. Lien has shown that the line profile of phonon associated transitions (phonon branches) with ΔJ higher than 2 is proportional to that of the phonon density of states.[39] The frequency shift of the phonon branch from the zero-phonon line is determined by the peak position of the phonon band. A broad feature at 2452.4 cm^{-1} was observed in the FTIR spectrum at 4 cm^{-1} resolution taken in a sample of 99.8% p-H_2 with an optical path of 11.5 cm as shown in Fig. 2. It is shifted from the $W_0(0)$ transition by about 42 cm^{-1}, consistent with the shift of other phonon branches from the zero-phonon lines.[15] We thus assigned this feature to be the phonon associated $W_R(0)$ transition of the $W_0(0)$ line. Ali and Tipping[40] have recently calculated various phonon branches in solid hydrogens based on the theory of Poll and Van Kranendonk.[41] The observed frequency shift of the

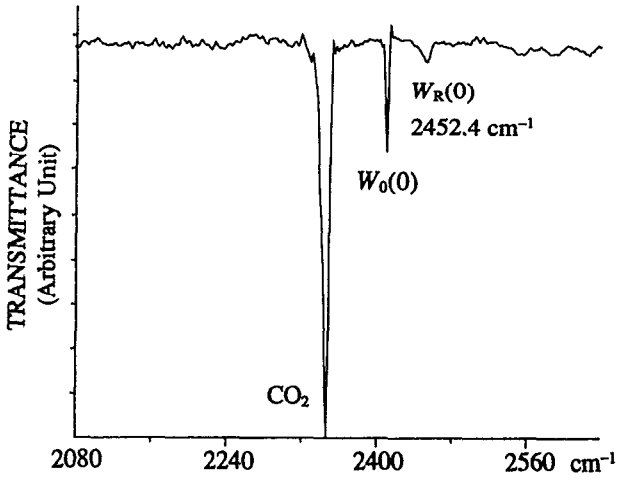

FIG. 2. FTIR spectrum of ~99.8% solid p-H_2 at 4 cm^{-1} resolution. The optical path is 11.5 cm. The broad feature at 2452.4 cm^{-1} was assigned to be the phonon sideband $W_R(0)$ transition of the $W_0(0)$ line. The absolute absorption of the $W_0(0)$ transition was about 0.25%. The strong absorption at left is due to trace amount of CO_2 in the N_2-purged optical path.

$W_R(0)$ transition suggests that this line may be due to doubly transverse optical phonon modes.[40]

C. $W_0(0)$ transition

In our preliminary studies reported in 1989, the $W_0(0)$ transition was observed at 2410.5384 cm^{-1} with a width of 0.003 cm^{-1} (90 MHz).[11] A small shoulder line at 2410.5242 cm^{-1} was also seen in the spectrum as shown in Fig. 3. Two possibilities giving rise to this shoulder line were anticipated—it was due either to the o-H_2 associated double transition or to the splitting of M levels in the $J = 6$ manifold by crystal field effect. In order to clarify this point, the effects of o-H_2 concentration and different planes of polarization of the infrared radiation on the intensity of the $W_0(0)$ line were studied.

Figure 4(a) shows the $W_0(0)$ line of a sample containing about 0.06% o-H_2 impurity. The main peak appeared at 2410.5349 cm^{-1}, and the shoulder was not seen suggesting that its intensity might be related to the o-H_2 concentration. Figure 4(b) shows the spectrum of the same sample taken under the same conditions as Fig. 4(a) except that the direction of polarization of the infrared radiation was rotated by ~90°. We found that the small shoulder line became much more prominent under this condition. Since the transition probability to different M levels in the excited state is determined by the orientation of the crystal and the direction of laser polarization, the drastic change in relative intensity reflects that these components may be due to different M states in the $J = 6$ level. We also observed a new line at 2410.5459

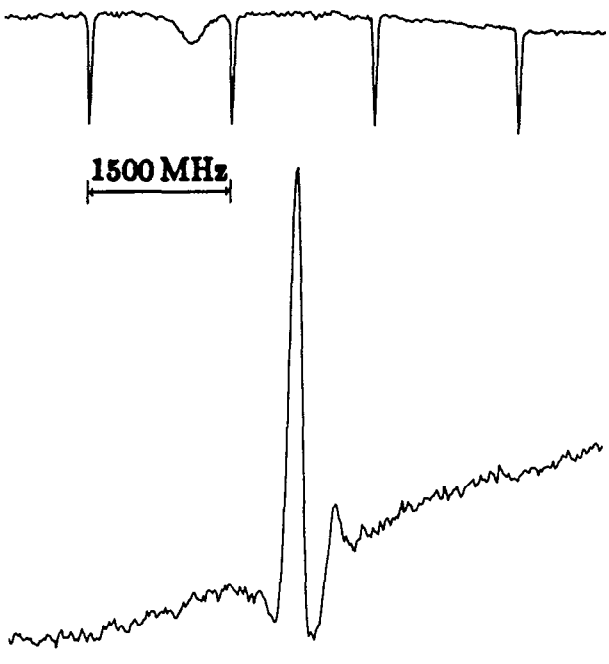

FIG. 3. The tone-burst spectrum (with 40 MHz RF frequency) of $W_0(0)$ transition using a difference frequency laser spectrometer, which was reported in Ref. 11. Frequency increases to the left. The main peak is at 2410.5384 cm^{-1}. An obvious shoulder line is observed at 2410.5242 cm^{-1}, at the low frequency side the main peak. The optical path is 11.5 cm and the sample contains 0.2% o-H_2. The broad feature in the top trace is the N_2O reference absorption. The sharp features in the top trace are Fabry–Perot interference patterns for frequency calibration.

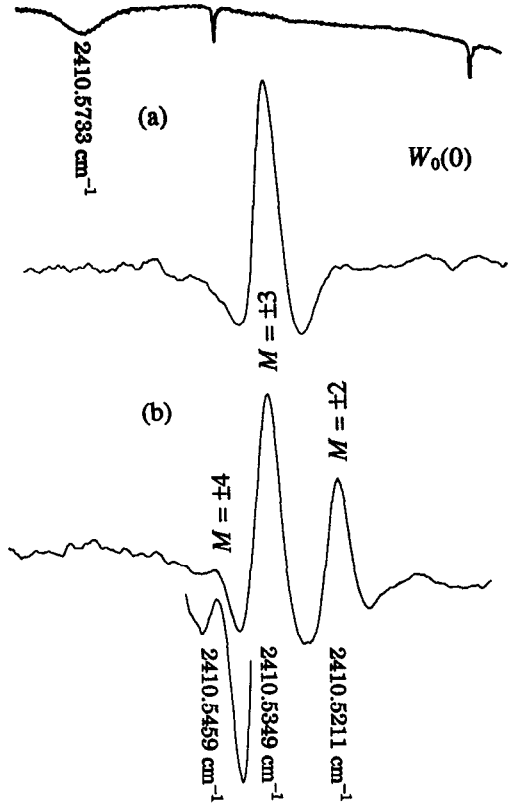

FIG. 4. Effect of the laser polarizations on the relative intensities of the components in the $W_0(0)$ transition. (a) The transition of a sample containing 0.06% of o-H_2 was recorded using a difference frequency laser spectrometer with 40 MHz RF tone-burst modulated at 6 kHz. The peak is at 2410.5349 cm^{-1} with HWHM 0.0023 cm^{-1}. The optical path is 11.5 cm. Spectrum (b) shows the same transition taken with laser polarization perpendicular to that used in (a). Two additional lines at 2410.5459 and 2410.5211 cm^{-1} are observed. The latter corresponds to the shoulder line in Fig. 3. The weak line at 2410.5459 cm^{-1} was magnified in the bottom trace. The drastic dependence of the relative intensity of these components on the laser polarization indicates some orientation of the crystal.

cm^{-1} appearing as a small shoulder. This triplet structure in the $W_0(0)$ transition agrees with the prediction from symmetry considerations discussed in Sec. II A.

The observed spectral width is smaller in the spectrum of the sample with lower o-H_2 concentration. The measured half-width at half-maximum (HWHM) is $\sim$70 MHz. Schoemaker and his co-workers have found a linear relation between the Raman linewidth of the $J=2$ roton and the concentration of o-H_2 impurity.[42,43] Our observation of sharper lines at lower o-H_2 concentration gives a similar trend, but the actual correlation has yet to be studied.

V. ANALYSIS OF SPECTRUM

Based on the predictions from group theory discussed in Sec. II A, both $U_0(0)$ and $W_0(0)$ transitions should split into triplets by crystal field interactions. However, only a single line was observed in the $U_0(0)$ transition indicating that in this case the splitting must be smaller than the linewidth due to homogeneous and inhomogeneous broadening. On the other hand, for the $W_0(0)$ line with a linewidth of an order of magnitude smaller, we are in fact observing the M splitting of the $J=6$ level as indicated by the clear dependence of the relative intensities on the infrared polarization.

The intensity of each M component of the $W_0(0)$ line was calculated using the dipole moment expression by Balasubramanian *et al.*[23]

$$\mu_\nu = 4\pi\sqrt{\frac{7}{15}}\,\frac{\alpha_{00}Q_{00}^{(6)}}{R_0^8}\sum_m C(617;m\nu m+\nu)\,Y_{6m}^{*}S_{7m+\nu}, \tag{10}$$

where $S_{7m+\nu}$ is the dimensionless lattice sum defined as

$$S_{7m+\nu} = \sum_\rho{}' \left[\frac{R_0}{R_\rho}\right]^8 Y_{7m+\nu}(\Omega_\rho).$$

$Q_{00}^{(6)} \equiv |\langle v=0,J=6|\mathcal{Q}^{(6)}|v=0,J=0\rangle|$ is the transition tetrahexacontapole moment, and α_{00} is the isotropic polarizability. Again the invariance of the lattice sum under operations in group $\mathcal{S}$ requires that $m+\nu = \pm 3$.

For $M=\pm 3$ state, the sA_2'' symmetry adapted wave function

$$|6,3\rangle_+ = \frac{1}{\sqrt{2}}\left[|J=6,M=3\rangle + |J=6,M=-3\rangle\right]$$

was used. The intensity was determined by the matrix element

$$\langle 0,0|\mu_0|6,3\rangle_+ = \frac{1}{\sqrt{2}}\left[\langle 0,0|\mu_0|6,3\rangle + \langle 0,0|\mu_0|6,-3\rangle\right].$$

For the $M=\pm 2$ state, the rotational wave functions belong to the sE' representation. We thus used the matrix elements

$$\langle 6,-2|\mu_{+1}|0,0\rangle \quad \text{and} \quad \langle 6,2|\mu_{-1}|0,0\rangle$$

to determine the intensity. The components μ_{+1} and μ_{-1} are the spherical components of the induced dipole moment. Since the $M=\pm 4$ state also belongs to the sE' representation, the intensity was calculated in a similar way except that the matrix elements become

$$\langle 6,-4|\mu_{-1}|0,0\rangle \quad \text{and} \quad \langle 6,4|\mu_{+1}|0,0\rangle.$$

The calculated intensity ratio of the three components is

$$I(|M|=4):I(|M|=3):I(|M|=2) = 6:40:45. \tag{11}$$

By comparing Figs. 4(a) and 4(b), we noticed that two peaks (at 2410.5459 cm^{-1} and 2410.5211 cm^{-1}) gain intensity from rotating the IR polarization. Since dipole moments $\mu_{\pm 1}$ cause both $M=\pm 2$ and ± 4 transitions, we thus assigned these two peaks as the $M=\pm 2\leftarrow 0$ at 2410.5211 cm^{-1} and $M=\pm 4\leftarrow 0$ at 2410.5459 cm^{-1} according to the calculated intensity [Eq. (11)]. The measured intensity ratio of these two lines is about 7 to 1, close to the calculated value of 45 to 6. The remaining peak at 2410.5349 cm^{-1} was assigned as the $M=\pm 3\leftarrow 0$ transition. This assignment is consistent with the theoretical prediction in the relative magnitude of splitting and the order of transition frequencies among the $|M|=2$, 3, and 4 levels discussed in Sec. II B. However the presence of the $|M|=3$ component in the case of perpendicular polarization is not yet understood.

Our new measurement of the transition frequencies differs from the previously reported values by about 0.0035 cm^{-1}.[11] This discrepancy can be ascribed to various sources: (1) the uncertainty in frequency measurement and (2) the shift of energy levels due to a different concentration of o-H_2 and a slight difference in lattice constants arising from different strains in the two samples. A more systematic study is necessary for further understanding.

Using the expressions of crystal field splitting of the localized roton discussed in Sec. II B, the phonon-renormalized Hamiltonian of the $J=6$ roton in hcp crystal can be written as

$$\tilde{\mathcal{H}}_c = \nu_0 + \tilde{\varepsilon}_{2c}C_{20}(\Omega) + \tilde{\varepsilon}_{4c}C_{40}(\Omega). \tag{12}$$

ν_0 is the angular independent transition frequency, and $\tilde{\varepsilon}_{2c}$ and $\tilde{\varepsilon}_{4c}$ are phonon-renormalized coupling constants. In fitting our experimental data using the above Hamiltonian, the value of one of the three parameters must be fixed. Schweizer, Washburn, and Meyer deduced, from the temperature dependence of the NMR signal, that $|\tilde{\varepsilon}_{2c}| = 0.0058$ cm^{-1}.[44] The data were fitted using both positive and negative values of $|\tilde{\varepsilon}_{2c}|$. It is seen from Table IV that the choice of the sign of $\tilde{\varepsilon}_{2c}$ has little effect on data fitting and a better fit of our experimental data was obtained by taking $\tilde{\varepsilon}_{2c} = -0.0058$ cm^{-1}. Assuming this value, ν_0 and $\tilde{\varepsilon}_{4c}$ were

TABLE IV. Experimental coupling constants of $W_0(0)$ transition.[a]

	$\tilde{\varepsilon}_{2c} = -0.0058$ cm^{-1}	$\tilde{\varepsilon}_{2c} = 0.0058$ cm^{-1}
$\nu_{obs}-\nu_{cal}$ (cm^{-1})		
$\|M\|=4$	0.0004	0.0006
$\|M\|=3$	−0.0007	−0.0010
$\|M\|=2$	0.0003	0.0004
σ(cm^{-1})	0.0009	0.0012
ν_0(cm^{-1})	2410.5243(7)	2410.5223(10)
$\tilde{\varepsilon}_{4c}$(cm^{-1})	−0.1224(64)	−0.1357(87)

[a] The data were fitted by assuming $|\tilde{\varepsilon}_{2c}| = 0.0058$ cm^{-1}, which was reported by Schweizer *et al.* (Ref. 42). Two sets of fitting were obtained by taking positive and negative values of $\tilde{\varepsilon}_{2c}$, respectively.

TABLE V. Frequencies, assignments, and linewidths of observed transitions.

Transitions	Frequency (cm^{-1})	Linewidth, HWHM (cm^{-1})	% o-H_2
$U_0(0)$	1167.1139 [a]	0.03 [b]	0.2
$W_0(0)$ $\|M\|=2$	2410.5211 [c]	0.0023	0.06
$\|M\|=3$	2410.5349 [d]	0.0023 [e]	0.06
$\|M\|=4$	2410.5459	... [f]	0.06
$W_R(0)$	2452.4 [g]	5.5 [g]	0.2

[a] In good agreement with Balasubramanian *et al.*, whose value was 1167.10 cm^{-1}.
[b] Sample temperature was ~4.2 K. Reported linewidth by Balasubramanian *et al.* for samples at 13 K was 0.125 cm^{-1}.
[c] Appeared as a shoulder at 2410.5242 cm^{-1} in the spectrum reported in Ref. 11.
[d] Reported frequency in Ref. 11 was 2410.5384 cm^{-1}, in samples with 0.2% o-H_2.
[e] Measured linewidth in Ref. 11 was 0.003 cm^{-1}, in samples with 0.2% o-H_2.
[f] Too weak for accurate measurement.
[g] Resolution of spectrum is 4 cm^{-1}.

determined to be 2410.5243 and -0.1224 cm^{-1}, respectively. The numerical value of $\tilde{\varepsilon}_{4c}$ obtained in the fitting is larger than the calculated value by about 10%. This discrepancy will be discussed in the next section.

The M splitting of the $U_0(0)$ transition was calculated using the constants determined from the $W_0(0)$ line. It is found that the energy shift of the $|M| = 2$, 3, and 4 levels of the $J = 4$ state are $+0.0109$, $+0.0236$, and -0.0133 cm^{-1}, respectively. Since the observed FWHM of the $U_0(0)$ line was 0.06 cm^{-1}, larger than the splitting of 0.0369 cm^{-1} between allowed transitions, it is consistent with the fact that the M splitting was not resolved for this transition.

A complete list of the transition frequencies, assignments and linewidths is presented in Table V.

VI. DISCUSSION

The discrepancy in the theoretical and experimental coupling constants may be ascribed to the effect of static and dynamic phonon renormalization.[30,31,45] A rigid hcp crystal was assumed in our calculations in Sec. II B. Because of the zero-point lattice vibration, the coupling constants calculated in Sec. II should be averaged over the phonon state. Since the displacement of H_2 molecules from the equilibrium site due to lattice vibration is so large (~18%), the correction due to lattice vibration can be very large in some cases. Van Kranendonk and Sears have illustrated that the combined effect of short-range interactions and phonon renormalization can give a correction of as much as a factor of two for $\tilde{\varepsilon}_{2c}$.[45] Silvera pointed out that the phonon-renormalized coupling constants can be increased by a factor of 2–10 from the unrenormalized quantities.[3] Harris has calculated the correction factors of static phonon renormalization for various types of interactions.[30] Extrapolating from the calculated renormalization factors by Harris,[30] we estimated the phonon-renormalization factor for ε_{4c} is about 1.2. More detailed theoretical studies on this problem are underway.

The sizable difference between the calculated and observed values of $\tilde{\varepsilon}_{2c}$ has been ascribed to the uniform distortion of the hcp crystal structure.[2] The stress and zero-point lattice vibration give rise to a homogeneous deviation from the ideal hcp structure, i.e., the ratio

$$\frac{c}{a} \neq \sqrt{\frac{8}{3}},$$

where $a = R_0$ and c is the vertical distance between each layer along the z axis of the hcp crystal. This deviation makes the contributions to $\tilde{\varepsilon}_{2c}$ become nonzero in the lattice sum for the first two shells. Such effect also changes the value of $\tilde{\varepsilon}_{4c}$ but its relative importance is much smaller.

Our high resolution spectrum of the $U_0(0)$ and $W_0(0)$ transitions has been interpreted by considering the crystal field splitting of the localized roton. To further examine the validity of this interpretation, we plan to study the structure of the $W_{1\leftarrow 0}(0)$ transition of solid H_2 using near infrared diode laser spectroscopy. According to the localized model, the crystal field splitting of the $W_{1\leftarrow 0}(0)$ line is scaled from those of the $W_0(0)$ line by a factor of

$$\frac{|\langle v=1,J=6|\mathcal{Q}^{(2)}|v=1,J=6\rangle|^2}{|\langle v=0,J=6|\mathcal{Q}^{(2)}|v=0,J=6\rangle|^2} \sim 1.2,$$

whereas the ratio of the splitting will be scaled by[11]

$$\frac{|\langle v=1,J=6|\mathcal{Q}^{(6)}|v=0,J=0\rangle|^2}{|\langle v=0,J=6|\mathcal{Q}^{(6)}|v=0,J=0\rangle|^2} \sim 0.33$$

in the delocalized roton model. In our preliminary study of the $W_{1\leftarrow 0}(0)$ line using FTIR spectroscopy,[11] no fine structure was observed in the spectrum at 0.05 cm^{-1} resolution.

The narrow widths of the $U_0(0)$ and $W_0(0)$ lines were unexpected. It is interesting to know how much of the width is due to homogeneous broadening and how much to inhomogeneous broadening. Based on the fact that we have observed even sharper features, on the order of 20 MHz, in the fundamental Q branch of the same sample,[16] it is likely that the widths of both pure rotational lines are dominated by homogeneous broadening. Studies of the spectral linewidth in solid hydrogen have been carried out only for the $\Delta J = 2$ excitation. Schoemaker and his co-workers have concluded, in a series of experiments, that the Raman spectral width of the $S_0(0)$ transition is homogeneously broadened by the dephasing of the $\mathbf{k} \approx 0$ roton in the $J = 2$ band.[42,43,46–48] They applied a scattering model to account for the phase relaxation process in which the Raman active $\mathbf{k} \approx 0$ roton is elastically scattered by the impurity molecules to a Raman inac-

tive $\mathbf{k}\neq 0$ roton of the same energy.[47] Homogeneous width due to radiation damping is also important for infrared absorptions because of the superradiant nature of coherent excitation in the solid state.[2] Following this idea, Van Kranendonk estimated the spectral width of the infrared active $S_0(0)$ transition to be $\sim 0.1\ \mathrm{cm}^{-1}$,[2] consistent with the observations by Buontempo *et al.*[14,49] using high resolution FTIR spectroscopy.

However, neither the scattering model nor the radiation damping can be applied to interpret our results. Unlike the $J=2$ roton, which travels through the crystal, the $J=4$ and $J=6$ rotons are relatively localized as we discussed in the preceding sections, and therefore the relaxation mechanisms of these rotons may be different from that of the $J=2$ roton. Phonon-induced processes may be possible mechanisms for the relaxation of localized excitons. Such processes usually have a temperature dependence. Statt and Hardy have extensively studied various one-phonon mechanisms contributing to the broadening of the o-H_2 pair spectrum.[50] Phonons couple to the exciton through EQQ and crystal field interactions. Because of the large mismatch between the Debye frequency ($\sim 90\ \mathrm{cm}^{-1}$) and the roton energy, the relaxation of the roton may involve multiphonon processes, which are much slower processes than one-phonon processes. In other words, the lifetime of high J rotons would be extraordinarily long simply because the routes of relaxation are inefficient. More studies are needed to quantitatively explain the spectral linewidths.

The excellent signal-to-noise ratio (>100) of the $W_0(0)$ transition suggests the possibility of observing transitions with even higher ΔJ, such as the $Y_0(0)$ transition with $\Delta J=8$, whose transition frequency is about $4050\ \mathrm{cm}^{-1}$. According to Ma, Tipping, and Poll,[51] the integrated intensity $\tilde{\alpha}$ of this transition relative to that of the $W_0(0)$ transition is given by

$$\frac{\tilde{\alpha}[Y_0(0)]}{\tilde{\alpha}[W_0(0)]} \sim 1.0\times 10^{-4}\,\frac{|\langle v=0,J=8|\mathcal{Q}^{(8)}|v=0,J=0\rangle|^2}{|\langle v=0,J=6|\mathcal{Q}^{(6)}|v=0,J=0\rangle|^2}.$$

Extrapolating the linewidths and multipole moments from those transitions with lower ΔJ, we estimate the $Y_0(0)$ transition would be about 10 MHz HWHM, and the transition 256-pole moment is about $0.189\ ea_0^8$. Using these values, we expect that the $Y_0(0)$ line would be $\sim 10^{-4}$ weaker (in $\Delta I/I$) than the $W_0(0)$ line. A more sensitive modulation/detection technique is being developed for studying this extremely weak transition. We hope the study of this transition can provide more information on the above-mentioned fundamental processes in the solid state.

One observation remains uninterpreted. The prominence of the $\Delta M=\pm 3$ transition in Fig. 4 for both laser polarizations could not be interpreted from our intensity calculations even if we considered a variety of orientations of the crystal and mixed crystal. Similar discrepancies in polarization dependence between the calculated and observed intensities have occurred for the $S_0(0)$ Raman spectrum[22] and the microwave spectrum of o-H_2 pairs.[52-54] Further systematic studies are planned to unravel this mystery.

In summary, the surprisingly sharp spectral widths observed in solid hydrogen allow us to study a variety of interesting phenomena in solid state physics, e.g., many-body radiation effects, exciton relaxation and line broadening mechanisms, many-body interactions, phonon–exciton coupling. Such studies will lead us to a better understanding of the solid state in general. As a long term goal, we plan to extend high resolution spectroscopic studies to other cryogenic solids and other neutral and ionic impurity species in solid hydrogen.

ACKNOWLEDGMENTS

We would like to thank M. -F. Jagod, B. D. Rehfuss, L. -W. Xu, C. M. Gabrys, and M. Rösslein for their assistance. This work was supported by the U. S. Air Force Contract No. F04611-86-K-0069 and the University of Dayton Research Center Award No. RI-68741X1F333615-87-C-2714. M. C. C. acknowledges a graduate scholarship from the United College, the Chinese University of Hong Kong.

[1] P. C. Souers, *Hydrogen Properties for Fusion Energy* (University of California, Berkeley, 1986).
[2] J. Van Kranendonk, *Solid Hydrogen* (Plenum, New York, 1983).
[3] I. F. Silvera, Rev. Mod. Phys. **52**, 393 (1980).
[4] See, for example, Chap. 5 of Ref. 2 and references therein.
[5] E. J. Allin, W. F. J. Hare, and R. E. MacDonald, Phys. Rev. **98**, 554 (1955).
[6] H. P. Gush, W. F. J. Hare, E. J. Allin, and H. L. Welsh, Can. J. Phys. **38**, 176 (1960).
[7] J. Van Kranendonk, Physica **23**, 825 (1957).
[8] J. Van Kranendonk, Physica **25**, 1180 (1959).
[9] J. Van Kranendonk, Can. J. Phys. **38**, 240 (1960).
[10] R. D. G. Prasad, M. J. Clouter, and S. P. Reddy, Phys. Rev. A **17**, 1690 (1978).
[11] M. Okumura, M. -C. Chan, and T. Oka, Phys. Rev. Lett. **62**, 32 (1989).
[12] Z. J. Kiss, Ph.D. thesis, University of Toronto, 1959.
[13] M. Treffler, A. M. Cappel, and H. P. Gush, Can. J. Phys. **47**, 2115 (1969).
[14] U. Buontempo, S. Cunsolo, P. Dore, and L. Nencini, Can. J. Phys. **60**, 1422 (1982).
[15] T. K. Balasubramanian, C. -H. Lien, K. N. Rao, and J. R. Gaines, Phys. Rev. Lett. **47**, 1277 (1981).
[16] M. -C. Chan, M. Okumura, C. M. Gabrys, L. -W. Xu, B. D. Rehfuss, and T. Oka, Phys. Rev. Lett. **66**, 2020 (1991).
[17] J. T. Hougen, J. Chem. Phys. **37**, 1433 (1962).
[18] H. C. Longuet-Higgins, Mol. Phys. **6**, 445 (1963).
[19] R. E. Miller and J. C. Decius, J. Chem. Phys. **59**, 4871 (1973).
[20] L. D. Landau and E. M. Lifshitz, *Quantum Mechanics: Non-Relativistic Theory*, 3rd ed. (Pergamon, New York, 1977).
[21] T. Oka, J. Chem. Phys. **47**, 5410 (1967).
[22] S. S. Bhatnagar, E. J. Allin, and H. L. Welsh, Can. J. Phys. **57**, 933 (1962).
[23] T. K. Balasubramanian, R. D'Souza, R. D'Cunha, and K. N. Rao, Can. J. Phys. **67**, 79 (1989).
[24] B. C. Carlson and G. S. Rushbrooke, Proc. Cambridge Philos. Soc. **46**, 626 (1950).
[25] R. B. Beuler and J. O. Hirschfelder, Phys. Rev. **83**, 628 (1951).
[26] M. E. Rose, J. Math. Phys. **37**, 215 (1958).
[27] R. A. Sack, J. Math. Phys. **5**, 260 (1964).
[28] C. G. Gray, Can. J. Phys. **46**, 135 (1968).
[29] C. G. Gray, Can. J. Phys. **54**, 505 (1976).
[30] A. B. Harris, Phys. Rev. B **1**, 1881 (1970).
[31] S. Luryi and J. Van Kranendonk, Can. J. Phys. **57**, 933 (1979).
[32] F. Mulder, A. Van der Avoird, and P. E. S. Wormer, Mol. Phys. **37**, 157 (1979).
[33] W. Meyer, Chem. Phys. **17**, 27 (1976).
[34] See Table 9, p. 42 of Ref. 2.
[35] K. -C. Ng, W. J. Meath, and A. R. Allnatt, Mol. Phys. **32**, 177 (1976).
[36] G. Guelachvili and K. N. Rao, *Handbook of Infrared Standards* (Academic, Orlando, 1986).
[37] A. S. Pine, J. Opt. Soc. Am. **64**, 1683 (1974).

[38] H. M. Pickett, Appl. Opt. **19**, 2745 (1980).
[39] H. -C. Lien, Ph.D. dissertation, Ohio State University, 1982.
[40] M. M. H. Ali and R. H. Tipping (private communication).
[41] J. D. Poll and J. Van Kranendonk, Can. J. Phys. **40**, 163 (1962).
[42] E. Goovaerts, X. Y. Chen, A. Bouwen, and D. Schoemaker, Phys. Rev. Lett. **57**, 479 (1986).
[43] C. Sierens, A. Bouwen, E. Goovaerts, M. De Mazière, and D. Schoemaker, Phys. Rev. A **37**, 4769 (1988).
[44] R. Schweizer, S. Washburn, and H. Meyer, J. Low Temp. Phys. **37**, 289 (1979).
[45] J. Van Kranendonk and V. F. Sears, Can. J. Phys. **44**, 313 (1966).
[46] M. Vanhimbeeck, H. De Raedt, A. Lagendijk, and D. Schoemaker, Phys. Rev. B **33**, 4264 (1986).
[47] X. Y. Chen, E. Goovaerts, and D. Schoemaker, Phys. Rev. B **38**, 1450 (1988).
[48] M. Leblans, A. Bouwen, C. Sierens, W. Joosen, E. Goovaerts, and D. Schoemaker, Phys. Rev. B **40**, 6647 (1989).
[49] U. Buontempo, S. Cunsolo, P. Dore, and L. Nencini, Can. J. Phys. **61**, 1401 (1983).
[50] B. W. Statt and W. N. Hardy, Can. J. Phys. **58**, 1341 (1980).
[51] Q. Ma, R. H. Tipping, and J. D. Poll, Phys. Rev. B **39**, 132 (1989).
[52] W. N. Hardy and A. J. Berlinsky, Phys. Rev. Lett. **34**, 1520 (1975).
[53] W. N. Hardy, A. J. Berlinsky, and A. B. Harris, Can. J. Phys. **55**, 1150 (1977).
[54] A. B. Harris, A. J. Berlinsky, and W. N. Hardy, Can. J. Phys. **55**, 1180 (1977).